

A Theoretical and Experimental Study of Failure Maps of Sandwich Beams with Composite Skins and Honeycomb Core

M. Sadighi^{i*}; A. A. Dehkordiⁱⁱ; R. Khodambashiⁱⁱⁱ

Received 31 January 2007; received in revised 27 January 2009; accepted 30 May 2009

ABSTRACT

Failure maps of sandwich panels such as beam, plate and shell are of great importance in designing such structures. In this paper, failure maps of sandwich beams with composite skin and honeycomb core are obtained. The effect of transverse shear in skins and core and the effect of double walls of honeycomb core have been taken into account. Shear deformation of skins and core are assumed to be linear. By minimizing the potential energy equation, the shear deformation coefficients of core and skins are obtained. Axial stresses in skins and core are obtained in terms of these coefficients. Core is assumed to have orthotropic properties.

Three point bending tests have been performed on some sandwich beam specimens. It is found that specimens for which failure load and its corresponding failure mode lie away from the boundary lines in failure map, there is a little difference between failure loads obtained from theories and experiments but this difference is more significant near the boundary lines due to combination of failure modes. In the case of transverse ribbon direction, the theoretical and experimental results are closer.

KEYWORDS

Sandwich beam, failure maps, honeycomb, composite skins and transverse shear stress.

1. INTRODUCTION

Sandwich panels are popular in high performance applications where weight must be kept to a minimum, for example aeronautical structures, high-speed marine craft and racing cars. They are made of two stiff, strong skins separated by a lightweight core (Fig.1.).

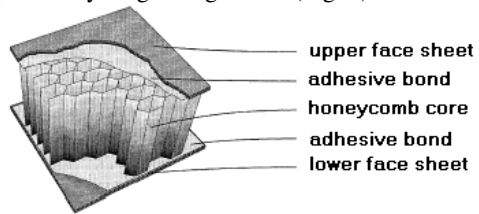


Fig.1. Honeycomb sandwich panel [3].

Typical modes of failure are skin yielding, skin wrinkling, intra-cell dimpling, core shear or local indentation (where the load is applied to the panel). The critical failure mode and the corresponding failure load depend on the properties of the skin and core materials,

on the geometry of the structure and the loading arrangement.

A comprehensive introduction to the subject of sandwich construction and the development of theoretical analyses up to 1969 is given by Allen [1]. Holt and Webber [2] summarized developments and analyzed the elastic behavior of honeycomb sandwich beams, assuming linear elastic behavior for the skin and a rigid core.

Many researchers have studied the mechanical properties of honeycomb cores in the past three decades. Gibson and Ashby studied the in-plane stiffness of honeycomb cores according to the bending model of cell edges [3]. Masters and Evans developed a theoretical model for predicting the in-plane elastic stiffness of honeycomb cores based on the deformation (namely flexure, stretching and hinging) of honeycomb cells [4]. Mechanical, thermal, and hygrothermal loading on a sandwich beam with a honeycomb core and laminated skins have been investigated by reference [5]. Wierzbicki and Abramowicz [6] presented a simple formula to predict the axial crash response of thin walled columns.

ⁱ* Corresponding Author, Associate Professor, Mech. Eng. Dept., Amirkabir University of Technology (email: mojtaba@aut.ac.ir)

ⁱⁱ M.Sc. Graduate, Mech. Eng. Dept., Amirkabir University of Technology

ⁱⁱⁱ M.Sc. Graduate, Biomedical Eng. Dept., Amirkabir University of Technology

Their method is based on the balance of external and internal work. This model was validated experimentally by Abramowicz and Jones [7]. Out-of-plane compressive and shear strengths of Nomex_® honeycomb were generally independent of the height and almost negligibly dependent on the cell geometry but were highly sensitive to the density of the honeycomb [8,9]. Yet, other work [10–12] suggested honeycomb shorter in height with smaller cell size offered higher values for both bare compressive and crush strengths and hence such structures have a better chance of remaining intact after transverse loading. Paik et al. [13] identified that an increase in wall thickness of a honeycomb core cell delayed the start of plastic deformation, offering a substantial increase in ultimate and crushing strengths.

In comparison to quasi-static, studies of impact loading suggested that dynamic effects were significant due to a combination of more complicated crushing patterns, inertia effects and material strain rate sensitivity. A study by Wu and Jiang [10] found that the final impact deformation of metallic honeycomb contained more irregular and extra folding mechanisms compared to those of the quasi-static. It was also revealed that the dynamic crush strength was significantly higher by between 33% and 74%. Similar studies [14, 15] also showed that a 40% and 50% increase, respectively, from the quasi-static to dynamic cases. The increase in the crushing strength could be attributed to a higher flow stress under dynamic loading, or was related to structural effects and is proportional to the mass density [16]. Failure mode maps have been derived by various authors for sandwich panels with flexible cores [17–18]. These authors concerned beams with ductile foam cores, making appropriate assumptions about the elastic and plastic behavior of the core and skin. The skins behave in a relatively simple manner, but the mechanical modeling of the core material, particularly for foams or honeycombs, is less straightforward. The response of the core to shear loading from the skins or loading normal to the plane of skins is required. The behavior depends both on the materials density used in the core and the ratio of the core density to that of the solid material constituting the core. Failure mode maps of sandwich beams with composite skins and honeycomb core have been obtained by Petras and Sutcliffe [19]. They did not take into account the effect of double walls in the core and skin shear.

In this paper loading under 3-point bending of sandwich beams made with composite skins and honeycomb core were considered. Under these conditions and considering the effect of shear stress in the skins and double walls of the honeycomb, failure mode maps of the beams are obtained. The overall procedure can be used to obtain failure mode maps for loading conditions other than 3 point bending. The predicted results are compared with the experimental results.

2. THEORY

In analyzing the composite skins like isotropic skins the displacement in y direction and the effect of γ_{yz} and γ_{xy} are neglected. The stress in z direction is lower than the stress in x direction and it is also ignored. With the above assumptions, the stress-strain relationships for a composite beam are rewritten as:

$$\begin{cases} (\sigma_x)_k = (\bar{Q}_{11})_k (\varepsilon_x)_k \\ (\sigma_{xz})_k = 2(\bar{Q}_{55})_k (\varepsilon_{xz})_k = (\bar{Q}_{55})_k (\gamma_{xz})_k \end{cases} \quad (1)$$

where \bar{Q}_{ij} are known as the reduced stiffness coefficients.

For calculation of stresses in each layer and the core shear, we need the values of displacements of each lamina. An element (dx) of a sandwich beam is shown after deformation in Fig.2. The index k indicates the number of layers, c is the thickness of the core and it is considered to be antiplane. If the shear deformation of core and skins are considered, the line $abcdefg$, which in the classical theory is assumed to remain perpendicular to the principal axes of the beam, moves to a new position $a'b'c'd'e'f'g'$. It is convenient to denote the angle $e'dz$ by $\lambda \frac{\partial w}{\partial x}$ and the rotation of layer k with respect to the vertical axes is denoted by $\mu_k \frac{\partial w}{\partial x}$.

μ_k, λ are the shear coefficients of skins and core.

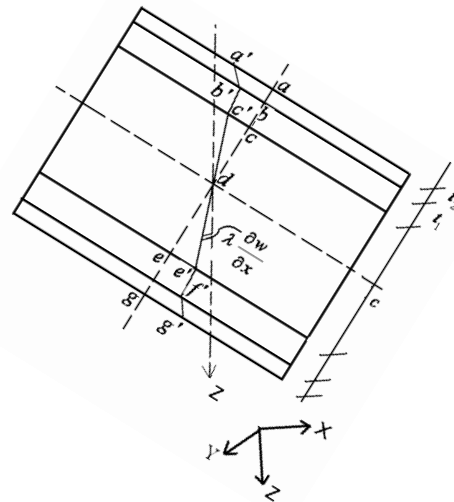


Fig.2. An element of the beam after deformation.

The displacement of the skins is assumed to be small. In deriving the strain energy equation of beam, axial strain in y and z directions and shear strains in xy and yz planes are neglected. Only the effect of shear deformation of skins in xz plane is taken into account. The strain in the skin is divided into two parts: membrane strain and

bending strain. Considering the deflection of the beam as Fourier series (for a simply supported beam) the strain energy equation of the sandwich beam with composite skins will become:

$$U + V = a_m^2 \left(\frac{m\pi}{L} \right)^2 \frac{L}{2} \left\{ \frac{G_c bc}{2} (1 - \lambda_s)^2 + \frac{E_c bc^3 \lambda_s^2}{24} \left(\frac{m\pi}{L} \right)^2 \right. \\ \left. + \sum_{k=1}^{NE} \frac{(\bar{Q}_{11})_k b \mu_k^2 t_k^3}{12} \left(\frac{m\pi}{L} \right)^2 + \sum_{k=1}^{NE} \frac{(\bar{Q}_{11})_k b t_k}{4} (c \lambda_s + \mu_k t_k + 2 \sum_{n=1}^{k-1} \mu_n t_n)^2 \right. \\ \left. \left(\frac{m\pi}{L} \right)^2 + \sum_{k=1}^{NE} (\bar{Q}_{55})_k b t_k (1 - \mu_k)^2 - \frac{P}{2} \right\} - a_m q_m \frac{L}{2}. \quad (2)$$

When the width of the beam is small compared with the thickness ($b < c$), the assumption of zero strain in the y direction is valid. Due to the low intensity of distributed load in z direction compared to the longitudinal stresses, the assumption of zero stresses in z direction is also valid.

In the above equation, a_m is the Fourier series coefficient which is analogous to the assumed deflection of the beam, q_m is the coefficient of the Fourier series of load, m is the Fourier series index and P indicates an axial load and b , c , t_k are width, core thickness and thickness of each layer of skin respectively.

If the system is under equilibrium, the potential energy ($U+V$) of the system with respect to the parameters μ_k , λ_s , a_m should be minimum. This needs a set of equation with $k+1$ unknowns (k unknowns for skin and one for core). In matrix form:

$$[K] \{ \mu \} = \{ 1 \} \quad (3)$$

Introducing parameters $\mu_{s,k}$, λ_s as known variables, the unknown coefficient a_m is obtained by minimizing the potential energy function with respect to a_m :

$$a_m = \frac{q_m L^2}{(P_{cr} - P)m^2 \pi^2} \quad (4)$$

In the above equation P_{cr} is the critical axial load which is obtained from the following equation:

$$P_{cr} = G_c bc (1 - \lambda_s)^2 + \frac{E_c b \lambda_s^2 c^3}{12} \left(\frac{m\pi}{L} \right)^2 \\ + \sum_{k=1}^{NE} \frac{(\bar{Q}_{11})_k b t_k}{2} (c \lambda_s + \mu_{s,k} t_k + 2 \sum_{n=1}^{k-1} \mu_n t_n)^2 \left(\frac{m\pi}{L} \right)^2 \\ + 2 \sum_{k=1}^{NE} (\bar{Q}_{55})_k b t_k (1 - \mu_{s,k})^2 \quad (5)$$

3. CALCULATING THE STRESS VALUES DUE TO TRANSVERSE LOADING

In the previous section the sandwich beam under transverse load $q(x)$ and axial load P was studied. Using

membrane and bending strains, the corresponding stresses in skins are derived as follows:

$$\sigma_{mem,k,l} = \frac{(\bar{Q}_{11})_k}{2} (c \lambda_s + t_k \mu_{s,k} + 2 \sum_{n=1}^{k-1} \mu_n t_n) a_m \left(\frac{m\pi}{L} \right)^2 \sin \frac{m\pi}{L} x \\ \sigma_{bend,k,l} = \frac{(\bar{Q}_{11})_k}{2} (2 z \mu_{s,k} - \mu_{s,k} (c + t_k) - 2 \mu_{s,k} \sum_{n=1}^{k-1} t_n) a_m \left(\frac{m\pi}{L} \right)^2 \sin \frac{m\pi}{L} x \quad (7)$$

Also, core shear stress is as:

$$\tau_c = G_c \gamma_c = G_c (1 - \lambda_s) a_m \left(\frac{m\pi}{L} \right) \cos \frac{m\pi}{L} x \quad (8)$$

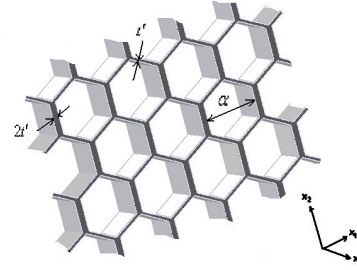


Fig.3. Hexagonal honeycomb.

Where τ_c and γ_c are the core shear stress and strain. It should be noted that the effect of axial load P should be taken into account when calculating the overall axial stresses in skins. The above equations can be used for plotting the failure maps of the beam or calculating its stresses and displacements. The procedure mentioned above could be used for calculation of deflection and stresses under any other loading conditions.

4. HONEYCOMB MECHANICS

To evaluate the failure mechanisms, stiffness and strength properties of the honeycomb core are required. Fig.3. illustrates a Nomex honeycomb structure. In particular walls normal to the X_1 direction have two layers of paper, while other walls have only a single layer.

For a first approximation the honeycomb Poisson's ratio can be taken as that of the solid material [3]:

$$\nu_{13} = \nu_{23} = \nu_s \quad (9)$$

The Young's modulus of the honeycomb in the out-of-plane X_3 direction is given by the rule of mixtures expression [3]:

$$\frac{E_3}{E_s} = \frac{\rho_c}{\rho_s} \approx \frac{8}{3\sqrt{3}} \left(\frac{t'}{l} \right) \quad (10)$$

where ρ_c and ρ_s are the density of honeycomb core and

the density of the materials which the honeycomb core made of it. In honeycombs, failure under out-of-plane compressive stresses occurs due to the fracture of cell walls or due to the elastic or plastic buckling of them [19]. For Nomex honeycombs, failure is due to a ‘crushing’ mechanism, initiated by elastic buckling and developing as a plastic buckling process.

Wierzbicki [18] gives an expression for the failure stress based on a plastic collapse model. For a honeycomb

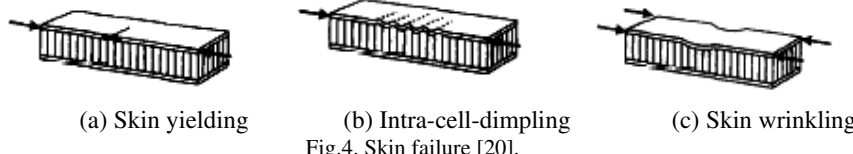


Fig.4. Skin failure [20].

Using simple mechanics models based on an array of regular hexagons and considering the double wall effect approximation, the shear strengths and shear moduli may be derived [3] as:

$$\begin{aligned} \frac{\tau_{31}}{E_s} &= 1.7 \left(\frac{\rho_c}{\rho_s} \right)^3 & \frac{G_{31}}{G_s} &= 0.375 \left(\frac{\rho_c}{\rho_s} \right) \\ \frac{\tau_{32}}{E_s} &= 2.6 \left(\frac{\rho_c}{\rho_s} \right)^3 & \frac{G_{32}}{G_s} &= 0.6 \left(\frac{\rho_c}{\rho_s} \right) \end{aligned} \quad (12)$$

Either G_{31} or G_{32} should be taken as the cores shear modulus depending on the orientation of the ribbon direction in the honeycomb. This anisotropy leads to a dependence of skin failure loads on the honeycomb orientation. Similarly the core shear strength depends on the honeycomb orientation.

5. FAILURE MODES

In the previous section maximum axial stress in the skins and shear stress in core were derived. These can be used to predict beam failure due to skin or core failure.

5-2. Core failure

The honeycomb sandwich structures loaded in bending may fail due to the core failure. Pertinent failure modes are shear failure or indentation by local crushing in the vicinity of loading point, as illustrated in Fig. 5.

5-1. Skin failure

According to section 2 maximum stresses in the skins can be derived by adding equations (6) and (7). This can be used to predict beam failure due to the skin failure modes: skin yielding, intra-cell dimpling or skin wrinkling, as illustrated in Fig. 4.

5-1-1. Skin yield

Failure occurs in the top skin due to skin yielding when the axial stress in skin reaches the in-plane strength of its material for loading along the beam axis.

$$\sigma_{mem.k.l} + \sigma_{ben.k.l} = \sigma_{fy} \quad (13)$$

with regular hexagonal cells this approach predicts the collapse strength:

$$\frac{\sigma_{cc}}{\sigma_{sc}} = 3.25 \left(\frac{\rho_c}{\rho_s} \right)^{5/3} \quad (11)$$

Honeycomb cores exhibit slight anisotropy in their out-of-plane shear strength and stiffness, due to the set of doubled walls.

5-1-2. Intra-cell-dimpling

A sandwich with a honeycomb core may fail by buckling of the skin where it is unsupported by the walls of the honeycomb (Fig. 4(b)). Simple elastic plate buckling theory can be used to derive an expression for the in-plane stress in the skins at which intra-cell buckling occurs as [19]:

$$\sigma_{fi} = \frac{2\bar{Q}_{11}}{1 - v_{fxy}^2} \left(\frac{2t'}{\alpha} \right)^2 \quad (14)$$

where α is the cell size (the diameter of the inscribed circle) of the honeycomb and E_f , and v_{fxy} are the elastic modulus and Poisson’s ratio of the skin for loading in the axial direction.

5-1-3. Skin wrinkling

Skin wrinkling is a buckling mode of the skin with a wavelength greater than the cell width of the honeycomb (Fig. 4(c)). Buckling may occur either in towards the core or outwards, depending on the stiffness of the core in compression and the adhesive strength. In practice, with 3-point bending, inward wrinkling of the top skin occurs in the vicinity of the central load location. By modeling of the skin as a plate on an elastic foundation, Allen [1] gave the critical compressive stress that result in wrinkling of the top skin as:

$$\sigma_{fw} = \frac{3}{(12(3 - v_{cxz})^2(1 + v_{cxz})^2)^{1/3}} E_f^{1/3} E_{3c}^{2/3} \quad (15)$$

where v_{cxz} is the out-of-plane Poisson’s ratio and E_3 is the out-of-plane Young’s modulus of the honeycomb core (see Section 4).

5-2-1. Core shear

Core shear failure occurs when the applied shear stress τ_c is equal to the shear strength τ_{cs} of the honeycomb core in this direction.

$$\tau_c = \tau_{cs} \quad (16)$$

Low density Nomex cores are particular susceptible to this failure mode.

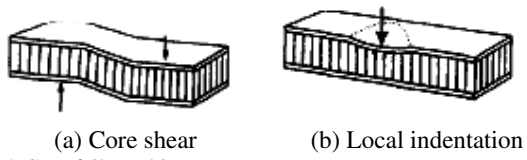


Fig.5. Core failure [20].

5-2-2. Local indentation (Core crushing)

Failure of sandwich panels in 3-point bending can occur at the load point due to local indentation. Failure is due to core crushing under the indenter. The bending stiffness of the skin and the core stiffness determine the degree to which the load is spread out at the point of application. This mode of failure has not been adequately modeled for honeycomb sandwich panels. To include this important failure mechanism, we use a simple empirical approach defined in handbooks of sandwich panel construction [19].

Table(1). Failure line loads corresponding to failure modes

$W_0 = \frac{\sigma_{fy}}{B_1}$	Skin yielding
$W_0 = \frac{2\bar{Q}_{11}}{(1 - v_{fy}^2)B_1} \left(\frac{2t}{\alpha}\right)^2$	Intra-cell-dimpling
$W_0 = \frac{B_3}{B_1} Q_{11}^{1/3} E_s^{2/3} \left(\frac{\rho_c}{\rho_s}\right)^{5/3}$	Skin wrinkling
$W_0 = \frac{A E_s}{B_2} \left(\frac{\rho_c}{\rho_s}\right)^3$	Core shear
$W_0 = 3.25 \sigma_{sc} \left(\frac{\rho_c}{\rho_s}\right)^{5/3} \delta$	Local indentation

We assume that the length of contact δ between the central roller and the top skin is known. It is further assumed that the load is transferred uniformly to the core over this contact length, so that the out-of-plane compressive stress σ_z , in the core is given by:

$$\sigma_z = \frac{W}{\delta} \quad (17)$$

Then failure is occurred when:

$$\sigma_z = \sigma_{cc} \quad (18)$$

where σ_{cc} is the out of plane composite strength.

The above approach is deficient in the three aspects of (i) the contact area must be estimated in some experimental way, (ii) load transfer from the roller to the core is oversimplified; this will depend on the relative skin and core stiffness, (iii) failure in the core will not be governed solely by the compressive stress in the core but will also be influenced by the local shear stress [19].

6. PLOTTING THE FAILURE MAPS

In the previous sections the failure mechanisms of sandwich beams with honeycomb core were explained. In

this section, the method of obtaining failure maps for certain beam geometry and failure mechanism are presented. Since local indentation at the loading point is also taken into account, the failure depends on loading conditions, roller radius R and area of contact δ . Failure load for each failure mode is obtained from equations presented in table (1). The failure load that is observed in the practice is the minimum value obtained from these equations. In that table, $A(2.6$ or $1.7)$ denotes the shear strength coefficient of equation (12) and depends on the double walls direction in honeycomb core.

$B_1 - B_3$ also depend on the skin and core properties which are defined as:

$$B_1 = \frac{(\bar{Q}_{11})_k}{L} \sum_{m=1}^{\infty} \frac{1}{P_{cr} - P} (2z \mu_{s,k} + c(\lambda_s - \mu_{s,k})) + 2 \sum_{n=1}^{k-1} (\mu_{s,n} - \mu_{s,k}) t_n \sin \frac{m\pi}{2} \quad (19)$$

$$B_2 = G_c \sum_{m=1}^{\infty} \frac{1}{P_{cr} - P} (1 - \lambda_s) \left(\frac{2}{m\pi}\right) \sin \frac{m\pi}{2} \quad (20)$$

$$B_3 = \frac{3}{(12(3 - v_{cz})^2 (1 + v_{cz})^2)^{1/3}} \quad (21)$$

Failure maps and failure loads could be obtained as a function of beam geometry and relative density of core.

Using equations presented in table (1) the maximum value of the load that can be supported by the beam with honeycomb core can be plotted against geometric parameters and relative density of core. These plots are the most useful one in designing sandwich beams. The plotting methods are presented in the following sections.

7. EXPERIMENTS

To validate the predicted results and comparing them with the classical theory presented in [19], a number of experiments have been performed for several sandwich beams with honeycomb core. The results of three point bending experiments have been presented here and they are compared with the theoretical results.

The sandwich panels were made of composite skins (with two layers of cross ply glass-epoxy and Nomex core). The mechanical properties of the panel are presented in table (2) and dimensions of specimens are depicted in table (3). Core with a density of 80 kg/m^3 , thickness 10, 20 mm and cell size of 3.175 mm was cut into beams with desired dimensions according to the ASTM standard [21]. The width of the beams was greater than the twice of the thickness of core and was chosen to 4 cm in all beams. In order to study the effect of double wall effects, two samples were prepared for each beam dimension and ribbons orientations were chosen to be perpendicular (one in longitudinal direction of beam and other perpendicular to it).



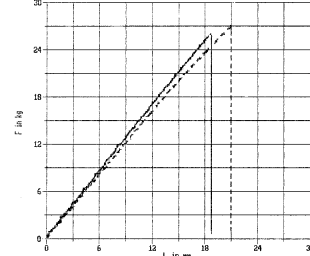
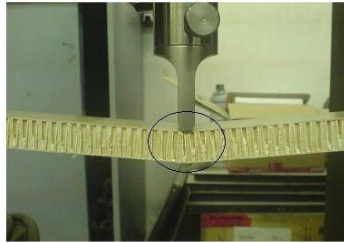
Fig.6. Three point bending test.

Table (2). Mechanical properties of the core and skins [19].

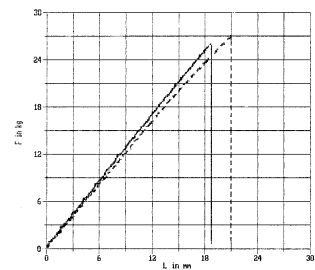
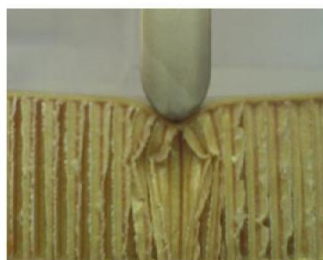
	Nomex core	Composite skins
Modulus of elasticity(GPa)	$E_s = 0.9$	$E_f = 20.5$
Shear modulus(GPa)	$G_s = 0.32$	$G_f = 4.2$
Compression strength(MPa)	$\sigma_{sc} = 80$	$\sigma_{fy} = 300$
Poisson's ratio	$\nu_s = 0.4$	$\nu_f = 0.17$

Table (3).Beam specimen dimension

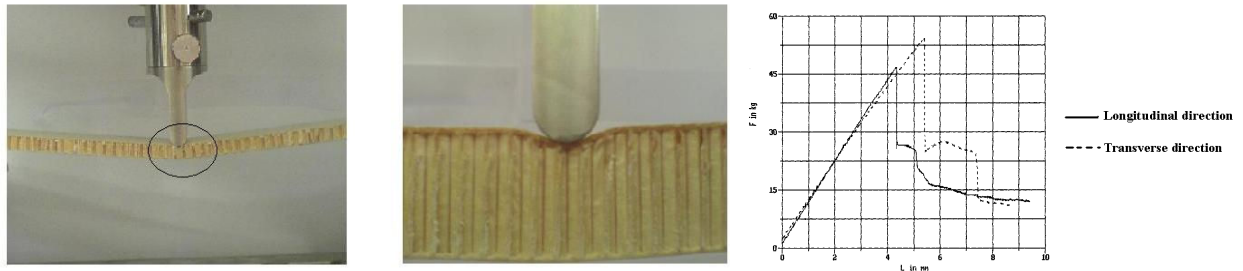
Length(mm)	700	700	500	500	350	350	250	250	175	175	125	125
Core thickness(mm)	18.9	8.96	18.9	8.96	18.9	8.96	18.9	8.96	18.9	8.96	18.9	8.96



(a) Skin yielding ($L = 620 \text{ mm}$, $C = 18.96 \text{ mm}$)



(b) Local indentation ($L = 300 \text{ mm}$, $C = 18.96 \text{ mm}$)



(c) Mixed failure ($L = 300 \text{ mm}$, $C = 8.96 \text{ mm}$)

Fig.7. Observed failure modes.

Table(4). Geometric characteristic and experimental result for specimens with 10 mm thickness

Core ribbon direction	Span Length(mm)	t/L	Measured failure load (N)	Predicted failure load (N)	(%)Error	Observed failure mode	Predicted failure mode
Longitudinal	500	1.04×10^{-3}	236	238.18	0.91	Face yield	Face yield
	400	1.3×10^{-3}	265.6	281.22	5.55	Face yield	Face yield
	300	1.73×10^{-3}	291.3	342.77	15.01	Local	Face yield
	200	2.6×10^{-3}	331.7	440.2	24.64	Local	Local
	150	3.47×10^{-3}	398.9	469.94	15.11	Local	Local
	100	5.2×10^{-3}	421.2	469.94	10.37	Local	Local
Transverse	500	1.04×10^{-3}	248.7	251.17	0.98	Face yield	Face yield
	400	1.3×10^{-3}	255.5	299.63	14.73	Face yield	Face yield
	300	1.73×10^{-3}	295.8	370	20.06	Local	Face yield
	200	2.6×10^{-3}	349.5	469.94	25.62	Local	Local
	150	3.47×10^{-3}	383.2	469.94	18.45	Local	Local
	100	5.2×10^{-3}	387.7	469.94	17.5	Local	Local

Table (5). Geometric characteristic and experimental result specimens with 20 mm thickness

Core ribbon direction	Span Length(mm)	t/L	Measured failure load (N)	Predicted failure load (N)	(%)Error	Observed failure mode	Predicted failure mode
Longitudinal	620	8.39×10^{-4}	385.4	465.17	17.15	skin yield	skin yield
	400	1.3×10^{-3}	432.4	539.5	19.85	skin yield	skin yield
	300	1.73×10^{-3}	458.2	640.09	28.14	Mixed	Local
	200	2.6×10^{-3}	416.8	657.92	36.64	Local	Local
	150	3.47×10^{-3}	515.4	657.92	21.66	Local	Local
	100	5.2×10^{-3}	504.1	657.92	23.38	Local	Local
Transverse	620	8.39×10^{-4}	410.1	501.64	18.25	Skin yield	skin yield
	400	1.3×10^{-3}	499.7	589.03	15.16	Skin yield	Skin yield
	300	1.76×10^{-3}	532.2	657.92	19.1	Mixed	Local
	200	2.6×10^{-3}	569.2	657.92	13.48	Local	Local
	150	3.47×10^{-3}	616.2	657.92	6.34	Local	Local
	100	5.2×10^{-3}	642.1	657.92	2.4	Local	Local

7-2. Test results

Figures 7(a)-7(c) show the typical failure mode of beams at the loading point (under the central roller). Also, load-displacement curve of these beams are plotted in Fig.7 for each failure mode. It should be noted that with the values of material properties used for core and skins,

the intra-cell-dimpling failure mode could not be predicted because according to equations (13) and (14) the minimum value of cell size in order to predict this failure mode should be 9 mm. For the majority of beams the failure occurred as local failure at the loading point and unpredictable behavior was seen in load-displacement curve after initial failure.

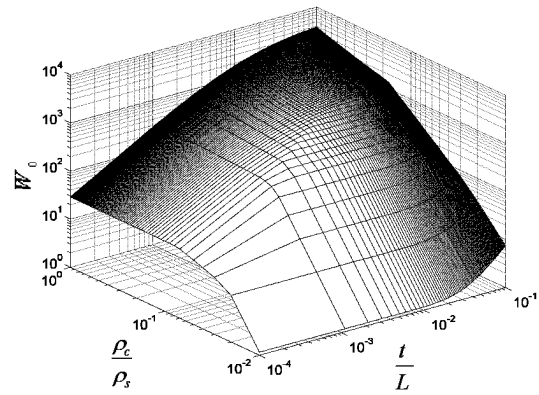
The average failure load and the corresponding failure mode are presented in tables (4 and 5). In table (5) the mixed failure mode refers to the simultaneous failure of core and skins. In this case failure mode of the structure could not be distinguished easily and the failure starts in one mode and is converted to other when the final failure occurs. This situation happens when the specimens according to their geometry are located near the boundary lines in the failure map. The predicted failure load according to table (4 and 5) and geometry and properties of core is plotted in Fig (8). The failure modes are obtained by projection of the intersection surfaces on the bottom surface and are plotted in Fig. (9).

7-3. Results and comparison

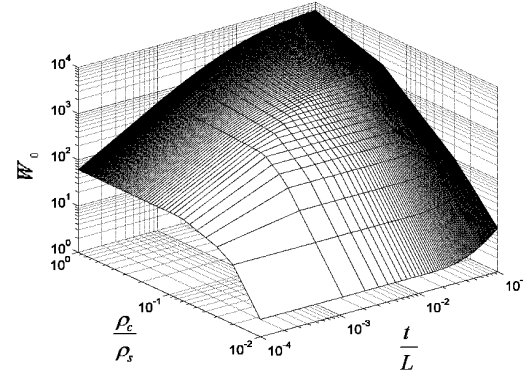
The experimental and theoretical values of failure load and corresponding failure mode for each of the two types of the cores are shown in Tables 4 and 5. Also, percent errors in the predicted load values are presented. The predicted error in the failure load of specimens with a length of 200 mm and core thickness of 8.96 mm is 24.64% when a mixture of skin yielding, skin wrinkling and local indentation happens at the loading point. This is the maximum value of predicted error which decreases with increasing the distance from boundary lines in the failure map. For example, the error for specimens with the length of 400 mm is estimated to be only 5.00 %. It is also seen that the predicted failure load for local indentation does not change with increasing the ratio of thickness of skin to the length of the beam while it is not observed by experimental results. For example, the error in failure load value for the specimens with a length of 100 mm is predicted to be 10.37% which is due to the uncertainty of theories in the modeling of this type of failure mode and error in calculating the contact area between the roller and the skin.

Plot of the failure load with respect to the thickness-to-length ratio and relative density of core material is presented in Fig 8. Generally, theories overestimate the failure load compared to the results obtained from the experiments, though at the maximum value (points at the boundary lines of failure map) the error is small. In other words at the points where mixed failure modes happen the difference between predicted values and experimental is considerable.

Also, the results are very close when the double walls are located transversely. It is evident from Fig.9 that with the used material properties and according to the thickness of specimens, the failure should only occur through skin yielding and local indentation at the loading point. (Indicated with stars in Fig.9 (a)).



(a) For totally thickness 10 mm



(b) For totally thickness 20 mm

Fig.8. Failure line load for various cores.

Generally speaking, the failure type of the most of the specimens is a mixed failure (combination of two failure modes) except those with small length. This is understood from Figs. 9(a and b) in which the failure points of most of the specimens are near the boundary lines and as mentioned earlier the failure mode and the corresponding failure load cannot be predicted for such points. For example, in long specimens failure occurs as a combination of skin yielding and skin wrinkling but final failure occurred due to the skin yielding which is also evident from Fig 9(a). The mixed failure mode is apparent for specimens' dimensions which are near the vertices of the figure (points of intersection of the three failure modes, for example specimens with a length of 400 mm).

In this condition the initial failure is skin wrinkling but final failure is combination of skin yielding and the local indentation. According to the geometry and properties of core local indentation was only predicted mode for this specimen.

The dash lines indicate the condition in which double walls of the honeycomb core are located transverse to the principal axis of the beam. It is found from the figures that the local indentation for transverse honeycomb ribbon direction is more likely to occur.

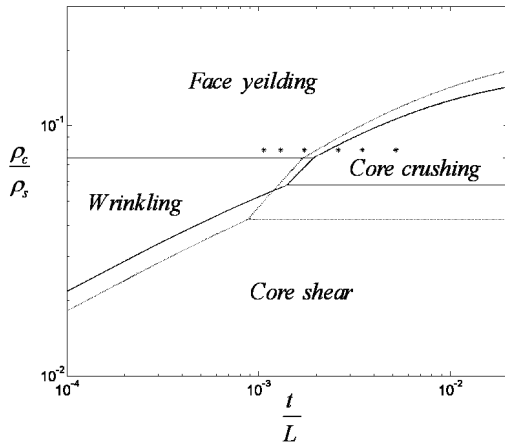
The difference between the experimental and theoretical failure loads of the structure increases with increasing the core thickness (Fig. 10) and in this case the maximum value of error occurs at the boundary lines. Failure maps of specimens with the total thickness of 20 mm are plotted in Fig. 9(b). In this case, the predicted failure mode is local failure at the loading point.

Generally skin wrinkling and local failure at the loading point occurs more often and therefore shear failure possibility is decreased

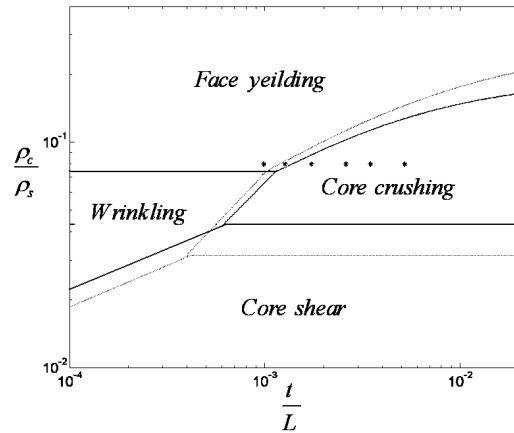
For this case similar to the case in Figure 9(a), single failure mode could not be observed but the results of a single failure mode can be used as a good approximation. For thicker cores it can be stated that the failure load has been increased.

Increasing of the failure load is accompanied with decreasing in the beam deflection (the bending stiffness of the beam was increased by a factor of 4 if the effect of core is not considered).

The failure load of the structure is plotted as a function of thickness-to-length ratio along with the empirical results in Fig.10. Away from boundary lines the failure load obtained from the experiments is closed to the theoretical results. For points near boundary lines a combination of failure modes occur which decreases the failure loads with respect to the individual failure modes. In the case of local failure at the loading point the error is large even for the points that are located away from boundary lines which indicate that this failure mode cannot be well predicted using contact area between the roller and skin.



(a) For totally thickness 10 mm

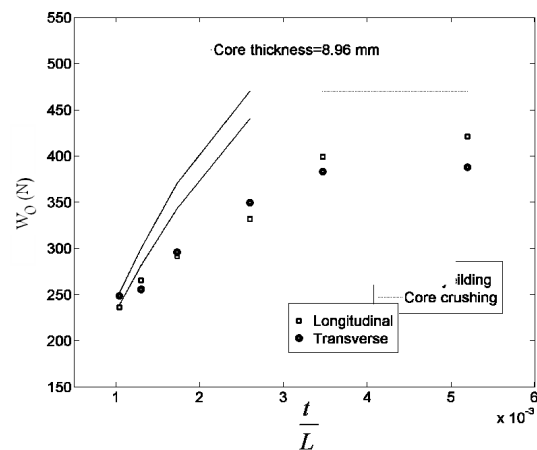


(b) For totally thickness 20 mm
Fig.9. Failure maps for various cores

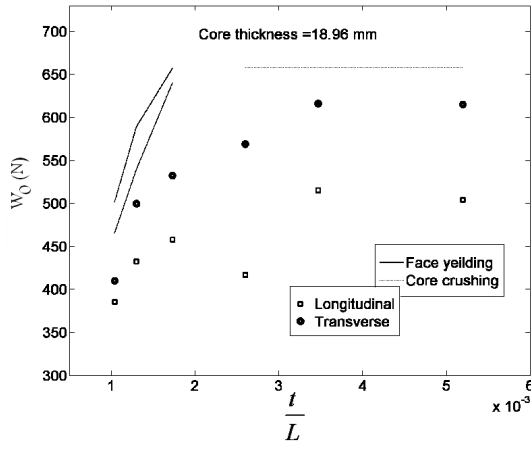
The results obtained for transverse double walls are more precise. This is shown in Fig.10 for skin yielding but it cannot be generalized to the local indentation. The main reason is the effect of double wall direction since the effect of direction of these walls is not taken into account in calculating the average core crushing strength (equation (11)). One of the major sources of error in failure load prediction and its corresponding failure mode is the existed error in the mechanical property values of the core.

7-4. Skin failure

In the long specimens, as predicted by theories, failure occurs at the skins. According to the material properties of the core the failure mode should be skin yielding. It could be said that the failure mode of the majority of the specimens are combination of failure modes near the boundary lines because the corresponding points are very closed to boundary lines and as a result the failure modes cannot be distinguished.



(a) For totally thickness 10 mm



(b) For totally thickness 20 mm

Fig.10. Comparison between the failure line loads

But the final failure of most of the specimens was skin yielding (Fig.7(a)). For example the initial failure for a specimen of length 620mm was local indentation and the final failure occurred suddenly.

7-5. Core failure

According to Fig.7 (b), the failure mode of the core was observed to be solely local indentation. This failure happened as the local buckling of honeycomb cells at the loading point. In some cases the local indentation is accompanied by skin failure but final failure was due to the core failure.

7-6 Skin wrinkling

According to equations (13) and (14) the critical cell size for which the failure mode changes from skin yielding to skin wrinkling can be calculated. This value was calculated to be 9 mm for the material used in the experiments. Since the cell size of all of the used specimens is 3.175 mm the skin wrinkling is not predicted at all. It should be noted that in this failure mode, contribution of double wall alignment to failure load is negligible which is due to the negligible effect of double walls in estimating the relative density of the core.

7-7. Effect of honeycomb ribbon direction

The specimens made in which double walls aligned with principal axis of the beam fail at lower loads compared to other specimens. This occurs in most of the specimens (Fig.7.). According to this figure the amount of absorbed energy before failure, is larger when double walls are aligned perpendicular to the principal axis of the structure.

Equation (11) gives the local indentation without considering the effect of double walls, so anisotropic properties of the core are not entered into the model for local failure. According to the intrinsic differences present in the load-displacement curve of beams with different

aligned double walls along the length of the beam, it is concluded that a more precise theoretical model which takes into account the effect of alignment of double walls with respect to principal axis of beam is needed in order to model this failure mode. Generally the obtained results for the cases of double walls located perpendicular to the principal axis of the beam are precise as are shown in Fig.10. But the results cannot be generalized to the local failure at the loading point. The main reason is due to the effect of double walls alignment in the core, which is not taken into account in calculating the mean wrinkling strength of the core (equation (11)).

8. CONCLUSION

Failure maps of sandwich beams with honeycomb core and composite skins have been plotted using equations that are derived for predicting the failure load of sandwich beams. In deriving these equations, the effect of transverse shear in skins, presence of double walls and ribbon direction are taken into account. To verify the results, a total number of 24 three point bending tests were performed on honeycomb sandwich beams with glass-epoxy skins and Nomex® core using Zwick machine. The length, core thickness and ribbon direction of beams were varied and the failure load and its corresponding failure mode along with the central deflection of beams were recorded and compared with theoretical results. The maximum deviation of theoretical results from experimental results ones near boundary lines of failure map (where different failure modes combine) but this does not cause considerable error. In the case of transverse ribbon direction, the theoretical and experimental results were closer when skin yielding occurs but this result was not observed in local indentation because the contact area between central roller and top skin could not be determined exactly.

9. ACKNOWLEDGEMENTS

The authors should thank the strength of material Lab. and Composite Lab. of mechanical engineering department of Amirkabir University of Technology for carrying the experiments. The authors are also grateful to Eng. Habib Pouriayevali for his valuable help

10. REFERENCES:

- [1] Allen HG. Analysis and design of structural sandwich panels. London: Pergamon Press, 1969.
- [2] Holt PJ, Webber JPH. Exact solutions to some honeycomb beam, plate and shell problems. *Journal of Strain Analysis* 1982; 17(I): 1-8.
- [3] Gibson LJ, Ashby MF. Cellular solids: structure and properties. 2nd ed. Cambridge, UK: Cambridge University Press; 1997.
- [4] Masters IG, Evans KE. Models for the elastic deformation of honeycombs. *Compos Struct* 1996;35:403-22.
- [5] Mukhopadhyay AK, Sierakowski RL. On sandwich beams with laminated facings and honeycomb cores subjected to hygrothermal loads: Part I. Analysis. *Journal of Composite Materials* 1990;24:382400.
- [6] Wierzbicki T, Abramowicz W. On the crashing mechanics of thinwalled structures. *J Appl Mech* 1983;50:727-39.
- [7] Abramowicz W, Jones N. Dynamic axial crashing of square tubes. *Int J Impact Eng* 1984;2:263-81.
- [8] Zhang J, Ashby MF. The out-of-plane properties of honeycomb. *Int J Mech Sci* 1992;34(6):475-89.
- [9] Zhang J. The mechanics of foams and honeycombs, PhD thesis, University of Cambridge, United Kingdom, 1989.
- [10] Wu E, Jiang WS. Axial crush of metallic honeycomb. *Int J Impact Eng* 1997;9(5-6):439-56.
- [11] Gotoh M, Yamashita M, Kawakita A. Crush behaviour of honeycomb structure impacted by drop-hammer and its numerical analysis. *Mater Sci Res Int* 1996;2(4):261-6.
- [12] Yasui Y. Dynamic axial crushing of multi-layer honeycomb panels and impact tensile behaviour of the component members. *Int J Impact Eng* 2000;24:659-71.
- [13] Paik JK, Thayamballi AK, Kim GS. The strength characteristics of aluminium honeycomb sandwich panels. *Thin-Walled Struct* 1999;35:205-31.
- [14] Zhao H, Gary G. Crushing behaviour of aluminium honeycombs under impact loading. *Int J Impact Eng* 1998;21(10):827-36.
- [15] Baker WE, Togami TC, Weydert JC. Static and dynamic properties of high-density metal. *Int J Impact Eng* 1998;21(3):149-63.
- [16] Wierzbicki T. Crushing analysis of metal honeycombs. *Int J Impact Eng* 1983;1(2):157-74.
- [17] Shenhar Y, Frostig Y, Altus E. Stresses and failure patterns in the bending of sandwich beams with transversely flexible cores and laminated composite skins. *Composite Structures* 1996;35: 143 - 152.
- [18] Triantafillou TC, Gibson LJ. Failure mode maps for foam core sandwich beams. *Materials Science and Engineering* 1987; 95:37-53.
- [19] A. Petras, M.P.F. Sutcliffe. Failure mode maps for honeycomb sandwich panels. *Composite Structures* 44 (1999) 237-252.
- [20] Ciba Composites, Duxford, England, Honeycomb Sandwich Design Technology. August 1995.
- [21] Anonymous, Method of flexure tests of flat sandwich structures. ASTM, 15.03 (C393-62) 1989.